Conflicting Roles of Flagella in Planktonic Protists: Propulsion, Resource Acquisition, and Stealth

S. S. Asadzadeh [1,*] J. H. Walther [2] and T. Kiørboe [1]

[1] *Centre for Ocean Life, National Institute of Aquatic Resources, Technical University of Denmark, DK-2800 Kongens Lyngby, Denmark*

[2] *Department of Civil and Mechanical Engineering, Technical University of Denmark, DK-2800 Kongens Lyngby, Denmark*

(Received 31 March 2023; accepted 9 June 2023; published 20 July 2023)

Flagellates are key components of aquatic microbial food webs. Their flagella propel the cell through the water and/or generate a feeding current from which bacterial prey is harvested, but the activity of the flagella also disturbs the ambient water, thereby attracting the flagellate's flow-sensing predators. Here we use computational fluid dynamics to explore the optimality and fluid dynamics of the diverse arrangements, beat patterns, and external morphologies of flagella found among free-living flagellates in light of the fundamental propulsion–foraging–predation-risk trade-off. We examine 5-μm-sized representative model organisms with different resource acquisition modes: autotrophs relying on photosynthesis and uptake of nutrient molecules, phagotrophs that feed on bacteria, and mixotrophs that employ both strategies. For all types, the transport of inorganic molecules is diffusion dominated, and the flagellum in autotrophic species therefore mainly serves propulsion purposes. Flagellates with a single, naked flagellum found among nonfeeding swarmer stages have a waveform (less than one wave) that is optimized for swimming and stealth but inefficient for feeding. Flagellates with a hairy flagellum typically have many waves, which optimizes swimming and stealth but is suboptimal for foraging, leading to a design trade-off. However, when compared with naked flagella, the presence of hairs allows a very efficient feeding current, making these primarily phagotrophic flagellates the most efficient and dominant bacterivores in the ocean. Autotrophic biflagellates have wave patterns optimized for both propulsion and foraging but conflicting weakly with stealth. Finally, the mixotrophic haptophytes are optimized for foraging, conflicting with both stealth and propulsion. This is largely due to the long, slender filament (haptonema) that improves prey collection but at the cost of stealth and propulsion. We use dimensional analysis to rationalize our findings. We conclude that phagotrophic flagellates must trade off stealth and propulsion for foraging efficiency, while in autotrophic flagellates stealth is traded off for propulsion and foraging efficiency.

DOI: 10.1103/PRXLife.1.013002

I. INTRODUCTION

Flagellates are few-micrometer-sized unicellular organisms equipped with one or a few flagella. They play a key role at the base of oceanic microbial food webs as the main consumers of bacteria and picophytoplankton and are themselves also important primary producers [1–4]. Flagellates have diverse resource acquisition strategies including autotrophy, relying on light and small inorganic nutrient molecules; phagotrophy, relying on prey capture (bacteria and picophytoplankton); and mixotrophy, employing both strategies. In all cases, the flagellum plays a central role in resource acquisition, by generating feeding currents from which prey can be harvested [5] and/or by propelling the cell to regions of high nutrient concentration [6]. At the same time, the beating flagellum disturbs the ambient fluid, thereby attracting the flagellates' flow-sensing predators, thus leading to a trade-off [7]. One may hypothesize that the design and activity of the flagellum are adapted to balance the conflicting needs of acquiring resources without the cell itself becoming a resource and that the large variation between species in the number, arrangement, waveform, and kinematics of the flagella and their equipment with hairs and vanes [8,9] represents different solutions to the propulsion–foraging–predation-risk trade-offs [10]. Other cell structures, such as a lorica (exoskeleton) [11] and haptonema (a long filament attached near the flagella in some species) may play a similar role. Despite the extensive focus on the role of the flagellum in propulsion and the fluid dynamics of swimming at low Reynolds number [12–14], there have been a limited number of studies [15,16] on the additional fundamental role of the flagellum in resource acquisition in free-living flagellates and on the significance of morphological variations. Here we use computational fluid dynamics (CFD) to investigate the connection between beat patterns and the morphology of the flagellum and its role in resource acquisition, propulsion, and stealth behavior. We investigate several uni- and biflagellate model organisms with different resource acquisition strategies, morphologies, and flagellar beat patterns. We describe these organisms using a common model that can accommodate all the observed flagellar wave patterns and characterize these by a few parameters (number of waves, curvature, amplitude, etc.) [17]. We next examine how the performance of the flagellum with respect to propulsion, resource acquisition, and

*sesasa@aqua.dtu.dk

Published by the American Physical Society under the terms of the Creative Commons Attribution 4.0 International license. Further distribution of this work must maintain attribution to the author(s) and the published article's title, journal citation, and DOI.

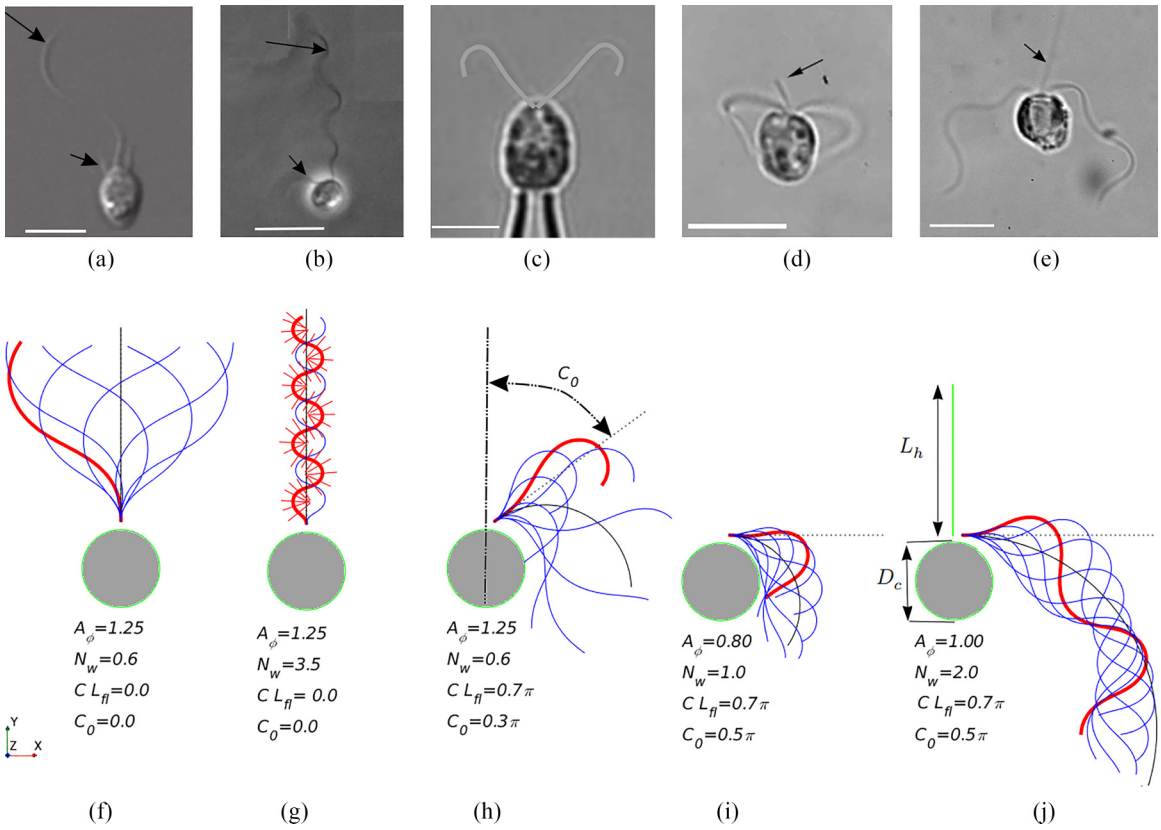

FIG. 1. Model organisms [(a)–(e)] and the associated model waveforms and morphologies [(f)–(j)]. (a) *M. brevicollis*, a predatory flagellate. The cell has one flagellum (long arrow) equipped with a vane (not visible) and a relatively short collar (short arrow) in this dispersal-swimming stage as compared with the feeding stage (Fig. S1). Image courtesy of Jasmine L. Mah. (b) *Pseudobodo* sp., also a predatory flagellate. The cell has a long and a short flagellum (long and short arrows, respectively), the long one bearing mastigonemes (hairs). (c) *C. reinhardtii*, a green alga with two active flagella. The cell shown here is held with a micropipette from below. Image courtesy of Kirsty Wan. (d) and (e) *P. parvum* and *P. polylepis*, respectively, are mixotroph haptophytes with two active flagella. The haptonema (arrow) is relatively short (∼3 μm) in *P. parvum*, while in *P. polylepis* it is much longer (∼20 μm). (f)–(j) Reconstruction of the flagellar waveform for different model organisms using dimensionless input parameters: A_ϕ, the amplitude of the angle; N_w, the number of waves; CL_{fl}, the maximum turning angle; and C_0, the turning angle measured from the symmetry line [dash-dotted line in (h)]. The blue curves show the flagellar waveform during the beat period, and the red curves correspond to the snapshots of the model organisms in (a)–(e). Prey capture happens on the cell surface and haptonema (green), and on the hairy flagellum for hairy flagellates. The rudimentary collar in *M. brevicollis*, the short flagellum in *Pseudobodo* sp., and the short haptonema in *P. parvum* are neglected in the model morphology. Scale bars, 10 μm.

stealth depends on wave parameters and morphologies, find optimum parameters for different morphologies, and identify critical trade-offs. We generally find good correspondence between observed flagellar beat patterns and those predicted for different resource acquisition strategies and morphologies.

II. METHODOLOGY

A. Model organisms

We consider flagellates (5–10 μm in cell size) with either one (uniflagellates) or two active flagella (biflagellates) as well as flagellates with a haptonema (haptophytes). The haptonema is a long, slender filament extending forward between the two flagella and can be used for collecting prey that arrives in the feeding current. For simplicity, we focus on species with a planar beat. To cover different cell types, we choose five model organisms each with a distinct waveform and morphology, namely, *Monosiga brevicollis*, *Pseudobodo* sp., *Chlamydomonas reinhardtii*, *Prymnesium parvum*, and *Prymnesium polylepis* [Figs. 1(a)–1(e)]. *M. brevicollis*, a choanoflagellate, is a predatory flagellate with one flagellum (∼20 μm in length), here shown in the nonfeeding swarmer stage [Fig. 1(a)]. The cell has also a thecate stage with a modified morphology (Fig. S1) with a longer collar filter (not simulated in this study) surrounding the flagellum that has a curvier waveform. *Pseudobodo* sp. is also a predatory flagellate. The cell has a long (∼25 μm) flagellum and a short (∼5 μm) flagellum, the long one bearing mastigonemes (hairs) extending in the beat plane [Fig. 1(b)]. The short flagellum is only active during prey handling but not during swimming or searching, and so we here group this species among the uniflagellates. During swimming the flagellum beats in a plane with many waves in a plane; in contrast, during feeding the flagellum beats in a complex three-dimensional pattern, and prey is perceived and captured by the flagellum [18] (Fig. S1). *C. reinhardtii* is a well-studied green alga (autotroph) with two active short flagella (∼10 μm). *P. parvum* and *P. polylepis*

TABLE I. Glossary of symbols.

Symbol	Description	Units
A_ϕ	amplitude of the angle	rad
α	hair orientation factor	
β	hair orientation factor	
c	concentration field	
C_0	constant turning angle of the flagellum	rad
C	characteristic of the dynamic component of the waveform	μm^{-1}
CL_{fl}	equal to $C \cdot L_{fl}$; the maximum turning angle of the flagellum	rad
D_c	diameter of the cell	μm
D_h	diameter of hairs	μm
D_{fl}	diameter of the flagellum	μm
δ	amplitude modulation factor	μm
A_E	maximum cross section (area of encounter)	μm^2
f	beat frequency	s^{-1}
F_u	thrust of the basic thrust unit	pN
$\bar{F}_{fl}$	force generated by flagellum in the swimming direction	pN
ϕ	angle of the tangent of the flagellum	rad
l	length of hairs	μm
L_{fl}	length of the flagellum	μm
L_h	length of the haptonema	μm
L_u	characteristic length of the basic thrust unit	μm
λ_ϕ	wavelength of the angle	μm
μ	viscosity	Pa s
n_s	unit normal vector on the organism's surface	
N	density of hairs	μm^{-1}
N_w	number of waves	
M	body mass of the organism	mgC
r_{cell}	radius of the cell	μm
r_p	radius of prey particles	μm
ρ	density	kg/m^3
s	arclength along the flagellum	μm
S_o	the organism's surface area	μm^2
Sh	Sherwood number	
$\boldsymbol{\sigma}$	stress tensor	Pa
P	instantaneous mechanical power expenditure by the organism	fW
$\bar{P}$	averaged mechanical power expenditure by the organism	fW
t	time	s
u	flow velocity	μm/s
$\bar{U}$	swimming speed	μm/s
U_u	characteristic speed of the basic thrust unit	μm/s
x_{fl}	x coordinate of material points on the flagellum	μm
y_{fl}	y coordinate of material points on the flagellum	μm

are mixotrophic haptophytes with two active flagella which are much longer (∼25 μm) in *P. polylepis* than in *P. parvum* (∼10 μm). The haptonema is relatively short (∼3 μm) in *P. parvum* (neglected here) but much longer (∼20 μm) in *P. polylepis*.

In the case of *M. brevicollis* the flagellum is equipped with a vane [9], and in the case of *Pseudobodo* sp. the flagellum has thick and tubular hairs. Note that vanes differ from hairs both morphologically and functionally. Hairs are extracellular tubular and rigid structures that protrude perpendicular to the flagellum [5,19] in the beat plane [8,20–22]. They reverse the direction of the feeding current as compared with that of a naked flagellum [23]. Vanes are a matrix of glycocalyx fibers that extend as a solid structure perpendicularly from the flagellar axis oriented perpendicular to the beat plane [9]. Unlike hairs, they augment the flagellum thrust in the same direction as that of a naked flagellum [24,25]. For *C. reinhardtii* the flagella are often observed with thin and short fibrous hairs with no apparent hydrodynamic functionality [26] and thus are neglected here.

B. Computational model

1. Model waveform and morphology

Our generic model flagellate has either one or two flagella of varying length L_{fl} with a spherical cell of diameter $D_c = 5$ μm and a haptonema of varying length L_h. All the parameters are listed in Table I.

To model the waveform of the diverse beat patterns in our model organisms, we follow the Geyer approach [27]. In 2016, Geyer *et al.* [27] showed that the breaststroke waveform of *Chlamydomonas* is a sinusoidal waveform traveling along

a circular arc, i.e., the waveform is a superposition of a static and a dynamic component. Such decomposition is also valid for our model organisms with a nonsinusoidal waveform, i.e., *C. reinhardtii*, *P. parvum*, and *P. polylepis*. The details of the beat analysis for these species, based on observations, are given in the Supplemental Material (Figs. S2, S3, and S4, respectively) [28]. *M. brevicollis* and *Pseudobodo* sp. have a sinusoidal beat pattern characterized only by the number of waves and amplitude [Figs. 1(f) and 1(g)]. The model for the waveform in nondimensional form is

$$\phi(s^*,t) = A_\phi(1-\exp(-s^*/\delta^*))\sin(2\pi ft - 2\pi N_w s^*) + (CL_{fl})s^* + C_0, \quad (1)$$

where $\phi(s^*,t)$ is the angle of the tangent of the flagellum with respect to the flagellar axis, $s^* = s/L_{fl}$ (where s is the arclength from the point of attachment on the cell body), and t is the time. The first term on the right-hand side of the above equation accounts for the dynamic component, where A_ϕ is the amplitude (of the angle), $N_w = \frac{L_{fl}}{\lambda_\phi}$ is the number of waves with wavelength λ_ϕ, f is the beat frequency, and $\delta^* = 0.1$ is an amplitude modulation factor dampening the amplitude where the flagellum is attached to the cell body. The second term accounts for the static component where CL_{fl} indicates the maximum turning angle of the flagellum (at its tip) in radians, and C_0 is a constant turning angle, orienting the flagellum with respect to the cell [Fig. 1(h)]. These two parameters effectively curve the flagella such that they pull the cell rather than push it. Finally, the flagellar beat is reconstructed using $x_{fl} = \int_0^s \cos\phi(s',t)ds'$ and $y_{fl} = \int_0^s \sin\phi(s',t)ds'$ [27].

In our model, the flagellum either is naked or has hairs (of a typical length of $l = 1.5$ μm) perpendicular to the flagellum and oriented in the beat plane [Fig. 1(g)]. The density of hairs in various flagellates is $N \geqslant 7$ μm^{-1}, and at these densities the hairs function as a flexible sheet [23]. Accordingly, in our current simulations of hairy flagellates, we choose $N = 7$ μm^{-1}. While it is unclear whether choanoflagellates have a vane also in the swarmer stage [9,29,30], we also consider cases where hairs are oriented perpendicular to the beat plane as a simplified representation of a vane. The orientation of hairs along the flagellum is given by $\tilde{\mathbf{r}} = \alpha\tilde{\mathbf{n}} + \beta\tilde{\mathbf{b}}$, where $\tilde{\mathbf{n}}$ and $\tilde{\mathbf{b}}$ are normal (in the beat plane) and binormal (perpendicular to the beat plane) unit vectors. In the vane configuration, $\alpha = 0.0$ and $\beta = 1.0$. In the case of hairy flagellates, to avoid physical interference, we have oriented the hairs slightly off the beat plane, i.e., $\alpha = 1.0$ and $\beta = 0.3\sin\phi(s,t)$. This slight modification in the model morphology allows a higher number of waves N_w as typically found in hairy flagellates [18,20].

2. Morphological and functional parameters

To explore the functionality of different waveforms and flagellar architectures, we define input parameters that define the waveform and output parameters that quantify the functionality of the flagellum. The dimensionless waveform parameters, based on our generic model, are $L^*_{fl} = \frac{L_{fl}}{D_c}$, A_ϕ, N_w, CL_{fl}, C_0, and $L^*_h = \frac{L_h}{D_c}$. Our output parameters are the thrust produced by the flagellum in a tethered cell $\bar{F}_{fl}$, the swimming speed $\bar{U}$, the normalized maximum cross section (encounter area) of the fluid disturbance ($\frac{A_E}{\bar{U}}$), and the Sherwood number (Sh). $\bar{F}_{fl}$ indicates the equivalent of a net force (thrust) produced by the flagellum, averaged over the beat cycle. $\bar{F}_{fl}$ ultimately gives rise to the flow of water past the cell or to relocation in a freely swimming cell. $\frac{A_E}{\bar{U}}$ is a measure of the extension of the fluid noise generated by the flagellum as an estimation of the predation risk towards flow-sensing predators. The maximum cross section [10] is defined as $A_E = \pi(\frac{3}{4\pi}V_{\max})^{2/3}$, where $V_{\max}$ is the maximum volume of the fluid around the flagellate (during the beat period) within which the fluid velocity exceeds a threshold value (e.g., $U_{th} = 50$ μm/s for prey detection [10]). The Sherwood number measures the advective enhancement of clearance rate due to flagellar activity over that of pure diffusion of prey particles or nutrient molecules toward the cell. With a dimensional analysis, we find the following generic relationships between input and output parameters (see Supplemental Material):

$$\bar{F}_{fl} = \sqrt{\mu L_{fl}\bar{P}}\,\Theta_F(L^*_{fl}, A_\phi, N_w, CL_{fl}, C_0, L^*_h), \quad (2)$$

$$\bar{U} = \sqrt{\frac{\bar{P}}{\mu L_{fl}}}\,\Theta_U(L^*_{fl}, A_\phi, N_w, CL_{fl}, C_0, L^*_h), \quad (3)$$

$$\frac{A_E}{\bar{U}} = \frac{L^2_{fl}}{U_{th}}\Theta_{EA}(L^*_{fl}, A_\phi, N_w, CL_{fl}, C_0, L^*_h), \quad (4)$$

$$\mathrm{Sh} = \frac{Q}{Q_D} = \Theta_Q(\bar{P}, r^*_p, L^*_{fl}, A_\phi, N_w, CL_{fl}, C_0, L^*_h), \quad (5)$$

where $Q_D = 4\pi D r_{\mathrm{cell}}$ is the clearance rate due to the pure diffusion of prey particles (with an effective diffusivity D), $r^*_p = \frac{r_p}{r_{\mathrm{cell}}}$ is the size ratio of prey to predator, and $\bar{P}$ is the mechanical power expenditure by the cell and flagellum (and haptonema) averaged over the beat cycle. The instantaneous power P is calculated:

$$P = \iint_{S_o} \mathbf{u}\cdot(\sigma\cdot\mathbf{n_s})dS, \quad (6)$$

where σ is the stress vector and $\mathbf{n_s}$ denotes the unit normal vector on the organism's total (flagellum + cell + haptonema) surface S_o pointing into the fluid.

According to Eqs. (2)–(5), the flagellum thrust and swimming speed both have a known relationship with the input power ($\bar{F}_{fl} \propto \sqrt{L_{fl}}$ and $\bar{U} \propto \sqrt{L_{fl}}$), noise ($\frac{A_E}{\bar{U}}$) is nearly independent of the power (Supplemental Material, Fig. S5), and the Sherwood number has an unknown dependence on the power (due to the nonlinearity of the advection-diffusion equation). Considering that simulations for calculating the Sherwood number require many beat cycles (∼20 cycles to reach a quasisteady state) and are computationally costly, we choose to run the feeding simulations for specific input power. However, for one case (uniflagellate with naked flagellum), we ran simulations with three values of power, and this shows that the pattern (i.e., the dependency of the number of waves) for the Sherwood number is independent of the power (Supplemental Material, Fig. S6). Thus the pattern of the flagellum thrust, swimming speed, noise, and Sherwood number are all independent of the power. For the sake of comparison, we show the results for all the output parameters using the same input power ($\bar{P} = 10$ fW), which is an estimate based on the metabolic rate for flagellates [31] (see Supplemental Material).

3. Computational fluid dynamics

We use computational fluid dynamics (CFD) to numerically solve the flow governing equations around the flagellum and the cell body in water with density of $\rho = 997$ kg/m^3 and viscosity of $\mu = 0.001$ Pa s. For the uniflagellates, the computational domain is a sphere of diameter 300 μm surrounding the flagellate. For biflagellates, we assume symmetry in the morphology and beat of flagella; this reduces the size of the computational domain to a semisphere including half of the flagellate [Fig. 1(h)], with symmetry boundary conditions (BCs) at the flat (symmetry) face of the domain. The surface of the flagellum (including hairs) and the cell body are subject to no-slip BCs, and the outer surface of the domain is subject to a uniform pressure BC. The domain is discretized on a finite-volume mesh and consists of polyhedral cells. The flagellum is moved using the morphing technique, which redistributes the finite-volume mesh corresponding to the flagellum motion. The discretized Navier-Stokes equations are solved using the commercial software STAR-CCM+ version 17.04.008. Simulations are conducted for both swimming and tethered organisms.

For the feeding simulations, we assume prey-size-dependent Brownian diffusivity according to the Stokes-Einstein relation $D = k_B T/(6\pi\mu r_p)$, where $k_B T$ is the Boltzmann energy at 16 °C, and prey concentration C satisfies the advection-diffusion equation [11,32,33]:

$$\frac{\partial c}{\partial t} + \mathbf{u}\cdot\nabla c = D\nabla^2 c, \tag{7}$$

where $c = C/C_\infty$ is the dimensionless concentration field, C_∞ is the concentration of the prey in the far field (outer boundary), and $\mathbf{u}$ is the flow velocity field. We assume a perfect absorber, where we set $c = 0$ in a thin volume around the cell with thickness $t_{\text{sink}} = r_p$, assuming that the prey (with radius r_p) is captured upon contact with the cell surface. For hairy flagellates, the flagellum also captures prey and is thus included in the capture zone.

III. RESULTS AND DISCUSSION

We vary the input parameters including, but not limited to, those of our model organisms to study the flagellate performance, i.e., thrust, swimming speed, fluid disturbance (predation risk), and resource acquisition. We show the results first for uniflagellates and then for biflagellates including haptophytes.

A. Uniflagellates

1. Naked and hairy flagella

Figure 2 shows the results for cells with a single naked, vaned, or hairy flagellum. The thrust produced by the naked flagellum in a tethered cell has an optimum when the flagellum has almost one complete wave, i.e., $N_w \simeq 1.0$; cf. Fig. 2(a). The addition of a vane increases the thrust but only slightly moves the optimum to $N_w \simeq 0.9$. When the flagellate is free to swim [Fig. 2(b)], the optimum waveform becomes less curvy ($N_w \simeq 0.4$). The optimum of less than one wave in the naked flagellum is consistent with the waveform in choanoflagellates where the flagellum is much less curvy in a free swimming cell [Fig. 1(a)] compared with attached cells of *M. brevicollis* [see also Figs. S1(a) and S1(b)] and for *Salpingoeca rosetta*; cf. Figs. 1 C and 1 G therein [30]. Note that in the tethered feeding stage, the cell also has a relatively long collar [Fig. S1(b)], neglected in this paper, which affects the magnitude of the produced thrust [24,34].

For the hairy flagellum, the pattern is different: The thrust increases with the number of waves. Note that our model morphology does not allow for reaching higher values of N_w (e.g., *Pseudobodo* sp. with $N_w = 3.5$) due to physical interference between hairs at the crest of waves. The increased thrust with more waves is consistent with the much curvier waveform of hairy flagellates as compared with that of a naked or vaned flagellum [compare Figs. 2(a) and 2(b)]. Thus the results show that while there are optima for cells with a naked or vaned flagellum, for hairy flagellates, the higher the number of waves, the better.

The dependency of the fluid noise ($\frac{A_F}{U}$) on the number of waves also differs between hairy flagella and naked or vaned flagella [Fig. 2(c)]: For the naked and vaned flagella, there is a local minimum at $N_w \simeq 0.4$, and the noise starts declining again at $N_w > 1.0$, while for the hairy flagellum, the noise decreases with the number of waves. Thus optima for thrust, speed, and stealth nearly coincide for both hairy and naked flagella, and there seems thus to be no conflict between these functions with respect to flagella waveform.

The feeding simulations [Fig. 2(e)] demonstrate that for foraging on small molecules with diffusivity $D \sim 4 \times 10^{-5}$ cm^2/s (autotrophs taking up inorganic nutrients), the enhancement of resource acquisition (Sherwood number) due to the feeding current is negligible [Fig. 2(f)]. These results are consistent with those of Tam and Hosoi [35] for the corresponding Péclet number of $\text{Pe} = \frac{\bar{U} r_c}{D} \sim 0.1$. Foraging on bacteria-sized prey particles (0.5 μm), however, is significantly enhanced by the feeding current, and much more so for hairy than for naked flagella. In the naked flagellum, the Sherwood number is almost independent of the number of waves, while for the hairy flagellate, the Sherwood number decreases with the increasing number of waves. That is, for hairy flagellates, there is a design conflict—or trade-off—between foraging on the one hand, and propulsion and predation risk on the other hand. Such a trade-off has been demonstrated empirically for flagellates [10], and our CFD simulations here suggest a mechanism underpinning such a trade-off.

2. Basic thrust unit

To rationalize the results for uniflagellates, it is instructive to consider that a flagellum comprises basic thrust units. That is, the flagellum is composed of repeating segments (units) that give rise to the produced thrust. The mechanism of function of these units differs between naked and hairy flagella [23]. The basic thrust unit for a naked flagellum is the straight part of the waveform, and it depends on the so-called drag-based thrust, the mechanism of which relies on the slenderness of the filaments of the flagellum [13]. The thrust of the basic unit F_u depends on the length (L_u) and velocity (U_u) of the unit, i.e., $F_u \sim \mu L_u U_u$. Neglecting the hydrodynamic interactions between the units and considering that there are $2N_w$ basic thrust units along the length of

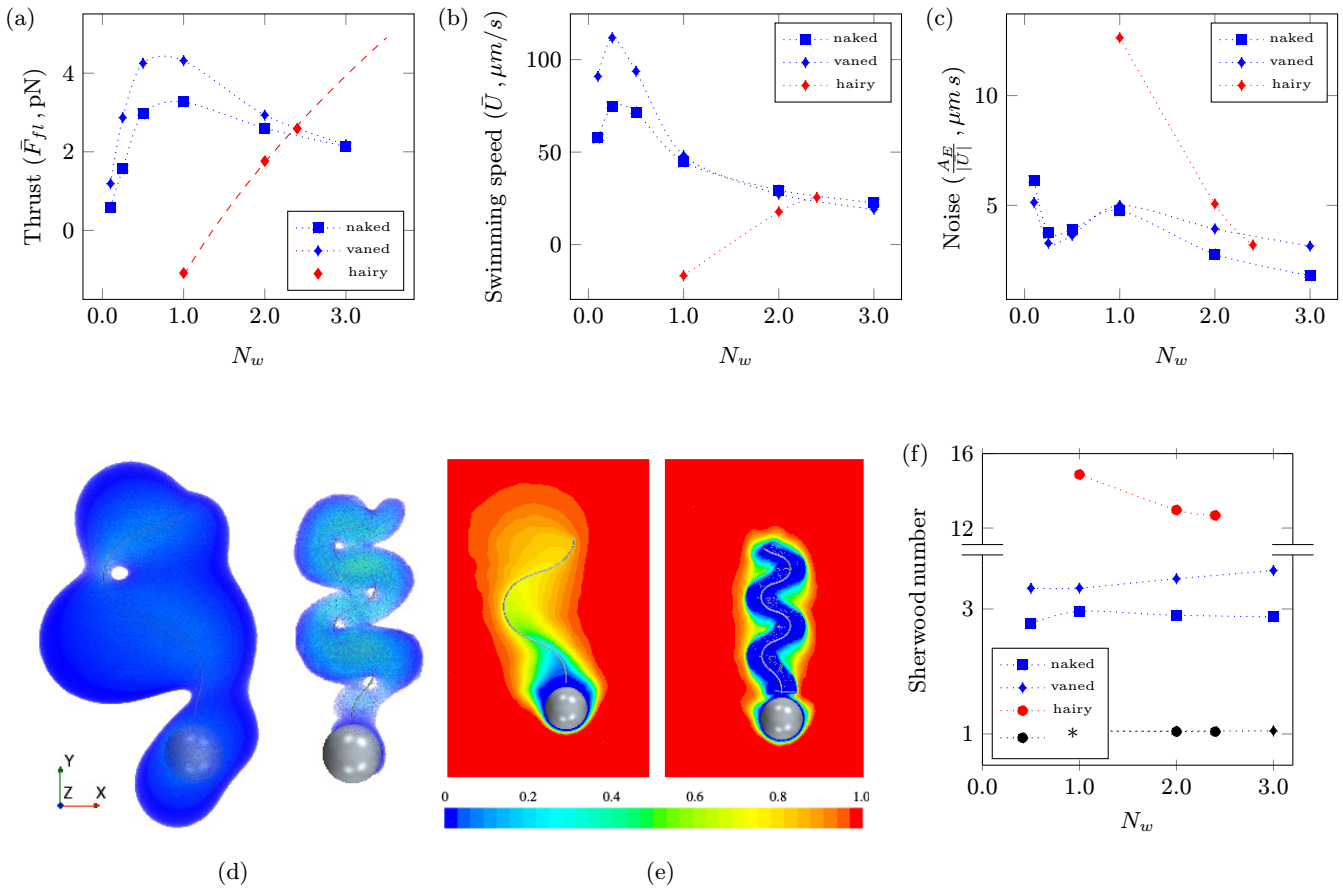

FIG. 2. CFD results for uniflagellates. (a) Flagellum thrust $\bar{F}_{fl}$ as a function of the number of waves N_w for cells with a naked flagellum ("naked"), a flagellum with a vane positioned perpendicular to the beat plane ("vaned"), and a flagellum with hairs positioned in the beat plane ("hairy"). The dashed curve is fitted to the CFD results for hairy flagellates (based on the mechanism of the produced thrust) with $\bar{F}_{fl} = a\sqrt{N_w} - b$, where a and b are positive constants. (b) Average swimming speed over a beat cycle as a function of the number of waves N_w, and (c) normalized extension of the fluid noise ($\frac{A_E}{\bar{U}}$) during a beat cycle as a function of the number of waves N_w. (d) and (e) Snapshots of the volume around the cell within which the fluid velocity exceeds the threshold velocity $U_{th} = 50$ μm/s (d) and of the concentration field (e), with $r_p^* = 10^{-1}$ corresponding to 0.5-μm prey-sized particles, for the cells with the naked (left) and hairy (right) flagellum. (f) The Sherwood number, the ratio of advective to diffusive transport, for $r_p^* = 10^{-1}$ as a function of the number of waves N_w. The asterisk denotes $r_p^* = 10^{-5}$ (corresponding to small molecules); for this r_p^* value the Sherwood number is nearly 1 for all cases indicating the predominance of the diffusion transport. Other relevant parameters: $N = 7\ \mu m^{-1}$, $l = 1.5$ μm, $A_\phi = 1.25$, $L_{fl}^* = 5$, and $\bar{P} = 10$ fW.

the flagellum, the thrust of the flagellum can be estimated as $\bar{F}_{fl} = 2F_u N_w \sim \mu L_u U_u N_w$, and the power consumption of the flagellum can be estimated as $\bar{P} = 2F_u U_u N_w \sim \mu L_u U_u^2 N_w$. Combining these two expressions, and assuming that the basic unit spans one-quarter of the wavelength $L_u = \frac{1}{4}\lambda_\phi$, yields

$$\bar{F}_{fl}\,|_{\text{naked}} \sim \sqrt{\mu L_{fl} \bar{P}}.$$

This expression suggests that if the hydrodynamic interactions among units were negligible, the produced thrust would be higher for a longer flagellum (also confirmed with CFD results; see Fig. S7) and should remain independent of the number of waves N_w. In reality, however, hydrodynamic interactions are important and tend to lower the value of the flagellum thrust, and thus the above expression gives the maximum possible flagellum thrust. The higher the number of waves, the closer the basic thrust units, and thus the higher the hydrodynamic interactions between the units, resulting in a decline in the thrust values with increased N_w; cf. Fig. 2(a). A faster decline is expected for higher values of A_ϕ, which makes the units closer (Fig. S7). On the other hand, the thrust also decreases as $N_w \to 0$, because the motion of the flagellum approaches reciprocality. This is consistent with the helical waveform of bacterial swimming where resistive force theory (neglecting hydrodynamic interactions) overestimates the produced thrust when helices have a small pitch [36]. The presence of a vane on the flagellum is not expected to alter the underlying mechanism, and thus the same behavior is expected for a vaned flagellum. Note that a vaned flagellum is often confined in some other (extra)cellular structures, such as a collar filter in the feeding stage of choanoflagellates, where the interaction between the collar and the flagellar vane is important for generating adequate flow into the collar [24] or for choanocytes in sponges [25,37]. Finally, it should be noted that the waveforms used in this paper are based on the flagellar deformation caused by the molecular

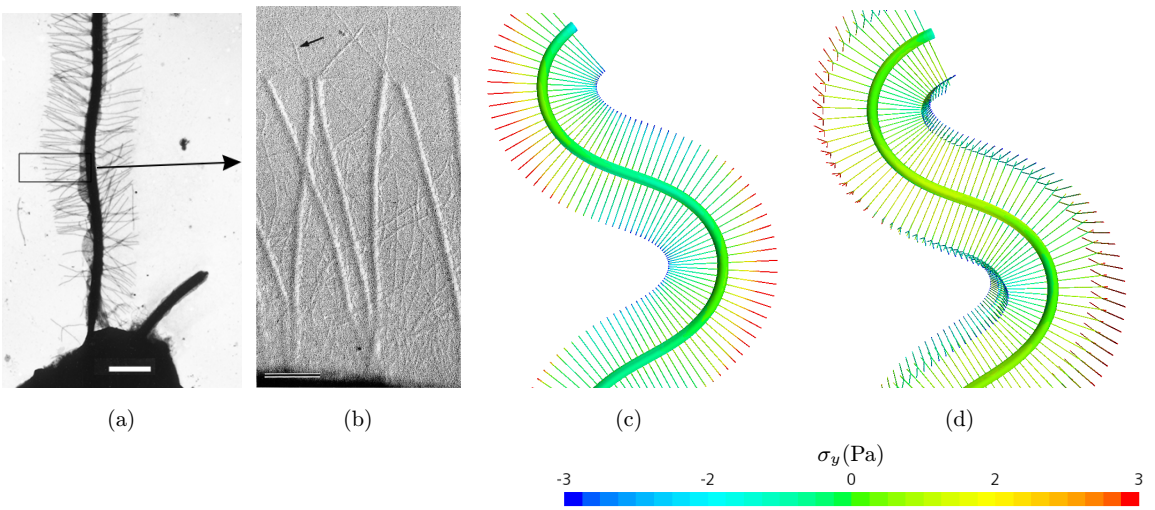

FIG. 3. Hair bundling and terminal filaments. (a) Hairs in flagellate *Melkoniania moestrupii* are often bundled together. (b) In addition, there are terminal filaments (arrow) on individual tubular hairs. (c) and (d) Spatial distribution of generated thrust σ_y without (c) and with (d) terminal filaments. Here, hairs have a length of $l = 0.9$ μm, and the terminal filaments have length $l_{tf} = 1.0$ μm and are positioned at distance $l_0 = 0.8$ μm on the hairs (measured from the attachment point of the hairs to the flagellum), with an arbitrary orientation of $\tilde{\mathbf{r}} = \tilde{\mathbf{n}} + 11\tilde{\mathbf{b}}$, where $\tilde{\mathbf{n}}$ and $\tilde{\mathbf{b}}$ are normal (in the beat plane) and binormal (perpendicular to the beat plane) unit vectors. The addition of the terminal hairs increases the thrust by 100% for the same kinematics and by 34% for the same power input. Scale bars in (a) and (b) are 1 and 0.2 μm, respectively. Other relevant parameters: $N = 7$ μm^{-1}, $A_\phi = 1.25$, and $L^* = 2.5$. Images courtesy of Robert A. Andersen.

motors (dyneins) [17,38]. If the flagellum could have any arbitrary deformation, then the optimum waveform may be "best described as a rounded sawtooth, for which the flagellum remains mostly straight except for narrow regions concentrating most of the bending deformation" (Ref. [33], p. 3). While this is consistent with the underlying mechanism, it may not be feasible since dyneins are curvature sensitive [17].

For a hairy flagellum, the basic thrust unit is the hairs at the crests of the wave, the mechanism of which relies on the hairs spanning different areas on the two sides of the flagellum at the crests of the wave [23]. For such units, $F_u \sim \mu A_\phi l U_u$ [23] and thus $\bar{F}_{fl} \sim \mu A_\phi l U_u N_w$ (neglecting the hydrodynamic interactions among units), and $\bar{P} \sim \mu A_\phi l U_u^2 N_w$. Therefore, for a hairy flagellum,

$$\bar{F}_{fl\,|\,\text{hairy}} \sim \sqrt{\mu l A_\phi N_w \bar{P}},$$

which shows that for a given length of hairs and input power, more thrust is produced with higher values of N_w [Fig. 2(a)] and also with higher A_ϕ, which may explain the often observed compressed waveform (higher A_ϕ; Fig. 1 therein [39]). Note that as N_w decreases (increasing λ_ϕ), the length of the unit ($L_u = \frac{1}{4}\lambda_\phi$) becomes longer than the "width" of the hairy flagellum (estimated as $2l$: one row of hairs of length l on each side of the flagellum), i.e., $\frac{1}{4}\lambda_\phi > 2l$ (or $N_w < \frac{L_{fl}}{8l}$), and this part of the flagellum, behaving like a slender object, produces a counteracting thrust. This negative thrust eventually dominates the (reduced) thrust produced by the basic units. Therefore it is expected that for a given input power, the flagellum thrust behaves as $\bar{F}_{fl} = a\sqrt{N_w} - b$, where a and b are positive constants that depend on the dimension of the flagellum [Fig. 2(a)]. This expression is, however, not valid in the extreme case where $N_w \to 0$ because, as for the naked flagellum, the beat pattern approaches reciprocal motion, with an expected zero thrust.

The above expression may explain the observation that hairy flagella often have many waves, as many as nine to ten, in contrast to a few waves in naked flagella; cf. Fig. 4 therein [20]. There is, however, a morphological trade-off between the length of the hairs and the number of waves due to the physical interference of the hairs for higher N_w. Hairy flagellates appear able to partially circumvent such a limitation, e.g., by hair bundling or adding terminal filaments to the end of the individual hairs; cf. Figs. 3(a) and 3(b). Simulation results including the terminal filaments in the model morphology show significant improvement in the produced thrust [Figs. 3(c) and 3(d)]. Also, many hairy flagellates have complex three-dimensional beat patterns, allowing for longer hairs and the potential to further enhance the produced thrust either by improving the basic units or by placing the basic units such that hydrodynamic interactions are minimal. Further exploration of such beat patterns is beyond the scope of this paper.

B. Biflagellates

1. *Short and long flagella*

Figure 4 shows the results of swimming and noise for different biflagellates. Similar to uniflagellates with a naked flagellum, the swimming speed [Figs. 4(a) and 4(b)] and noise [Figs. 4(d) and 4(e)] for these biflagellates show optimum values for N_w. This behavior indicates a drag-based thrust mechanism for these (naked) biflagellates as well. The optimum point, however, depends on other waveform parameters (e.g., C_0 and A_ϕ); for the cases with short flagella ($L^*_{fl} = 2$), the optima in the swimming speed correspond well with the beat pattern of our model organisms *C. reinhardtii* and *P. parvum* with dimensionless parameters of $A_\phi = 1.25$, $N_w = 0.6$, and $C_0 = 0.3\pi$ and of $A_\phi = 0.80$, $N_w = 1.0$, and $C_0 = 0.5\pi$, respectively. This indicates that *C. reinhardtii*

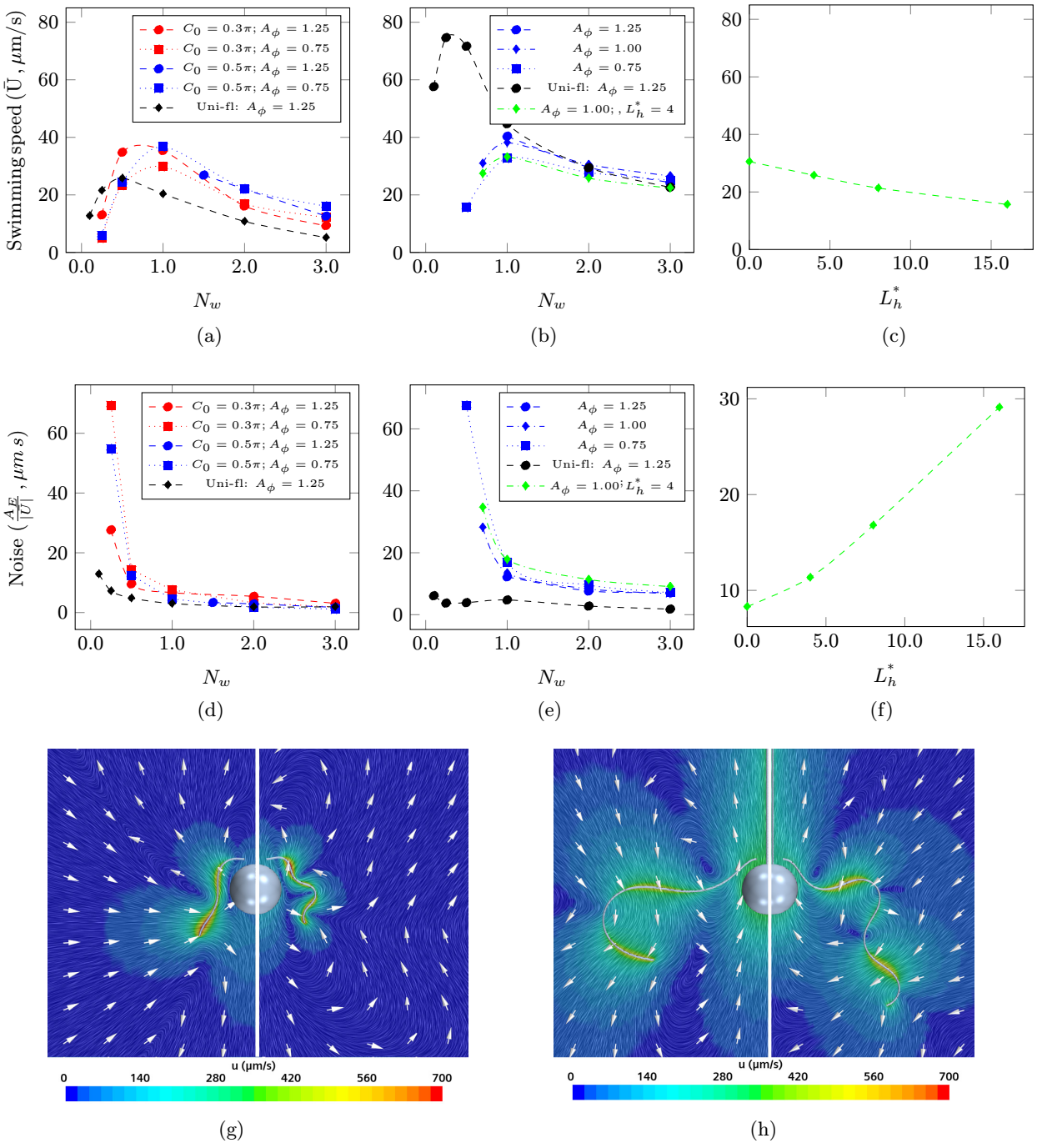

FIG. 4. CFD results for biflagellates' swimming and noise. Swimming speed (a) and normalized noise (d) as a function of number of waves N_w for the cases with short flagella ($L_{fl}^* = 2$) and no haptonema, and swimming speed (b) and normalized noise (e) as a function of number of waves N_w for the cases with long flagella ($L_{fl}^* = 5$) and no haptonema. For comparison, results for uniflagellates (uni-fl; black) and cells with haptonema (green) are also added. (c) and (f) Effect of length of the haptonema L_h^* on swimming and noise with parameters $L_{fl}^* = 5$ and $N_w = 5$. (g) and (h) Snapshots of the velocity field for freely swimming flagellates with short flagella [$L_{fl}^* = 2$ (left, $N_w = 1$; right, $N_w = 2$)] (g) and long flagella [$L_{fl}^* = 5$ (left, $N_w = 1$; right, $N_w = 2$)] (h). Other relevant parameters: In (g), $A_\phi = 0.75$, $C_0 = 0.5\pi$, and $L_h^* = 0.0$; in (h), $A_\phi = 1.00$, $C_0 = 0.5\pi$, and $L_h^* = 4.0$. For all cases, $CL_{fl}^* = 0.7\pi$ and $\bar{P} = 10$ fW.

and *P. parvum* are efficient swimmers. The noise declines very rapidly up to $N_w \sim 0.5$ and remains near constant for $N_w > 0.5$. In addition, biflagellates with short flagella appear to be much more efficient swimmers as compared with uniflagellates with the same dimension [i.e., $L_{fl}^* = 2$; black curves in Figs. 4(a) and 4(d)] and the same input power. These results are consistent with those of Tam and Hosoi [33], who showed that the optimum waveform resembles a so-called "breaststroke" beat (close to the waveform of *C. reinhardtii*), which is thus more efficient than biflagellates with a so-called

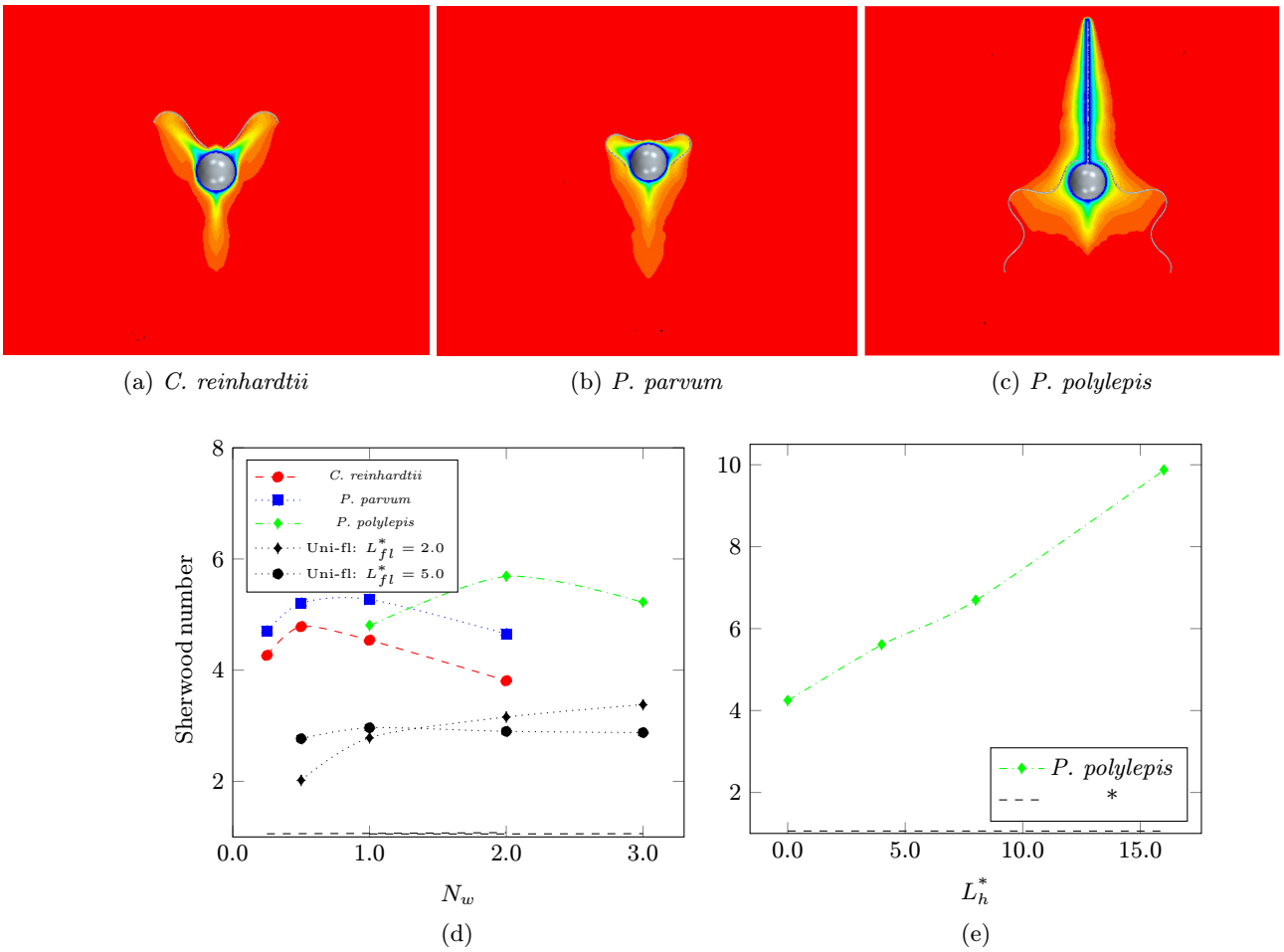

FIG. 5. CFD results for biflagellates' feeding. (a)–(c) Snapshots of the concentration field (with $r_p^* = 10^{-1}$) with parameters corresponding to those of *C. reinhardtii* (a), *P. parvum* (b), and *P. polylepis* (c). (d) Variation in Sherwood number as a function of the number of waves N_w for the three model organisms feeding on ∼0.5-μm-sized prey particles ($r_p^* = 10^{-1}$). For comparison, results for uniflagellates with long and short flagella are added as black dotted curves. The black dashed line shows the Sherwood numbers for small molecules ($r_p^* = 10^{-5}$, denoted in the key with an asterisk). (e) Effect of the length of the haptonema on the Sherwood number. For all cases, $\bar{P} = 10$ fW.

"undulatory stroke" (the stroke of each flagellum close to the waveform of *M. brevicollis*). Considering a cilium (flagellum) near a wall, Eloy and Lauga [40] similarly showed in 2012 that a breaststroke beat maximizes the transport of the surrounding fluid at a minimum energetic cost.

For the cases with long flagella [$L^*_{fl} = 5$ and $C_0 = 0.5\pi$; Figs. 4(b), 4(e), and 4(h)], the optima in the swimming speed occur near $N_w = 1.0$, while the noise drops rapidly until $N_w = 1.0$ and stays near constant above this value, also when the haptonema is added [green curves in Figs. 4(b) and 4(e)]. Thus *P. polylepis* ($A_\phi = 1.00$ and $N_w = 2.0$) is an inefficient but quiet swimmer. Moreover, adding a haptonema appears disadvantageous for the flagellate in terms of swimming speed and noise; the longer the haptonema, the more adverse the effect [Figs. 4(c) and 4(f)]. *P. polylepis* is also a very inefficient swimmer when compared with a uniflagellate with the same input power and length of the flagellum [i.e., $L^*_{fl} = 5$, black curves in Figs. 4(b) and 4(e)]. As described below, these mixotrophic biflagellates with a long haptonema have flagellar waveforms that appear to be optimized for resource acquisition.

To investigate the feeding performance, we vary the number of waves and the length of the haptonema around the parameters of our biflagellate model organisms. Figures 5(a)–5(c) show snapshots of the concentration field corresponding to that of *C. reinhardtii*, *P. parvum*, and *P. polylepis* for a prey-to-predator ratio of $r_p^* = 0.1$. Note that since for *P. polylepis*, the haptonema also contributes to prey capture [41], it is included in the capture area together with the cell body. The beat patterns of all three biflagellates have different local optima for feeding that, however, largely correspond to the waveforms found in the model organisms [Fig. 5(d)]. Interestingly, the mixotroph *P. parvum* outperforms the autotroph *C. reinhardtii*, and the inefficient swimmer haptophyte *P. polylepis* shows an efficient feeding performance when compared with *C. reinhardtii* and *P. parvum*. Furthermore, the feeding performance improves as the haptonema becomes longer [Fig. 5(e)]. In fact, in some haptophytes, the haptonema is long, 20 cell diameters or more (cf. Ref. [42]; $L^*_h \sim 20$), potentially making these cells efficient feeders, but at the cost of noisy, inefficient swimming. However, a long haptonema has other advantages since in some species the haptonema may

sense the fluid disturbance of an approaching predator, allowing the cell to respond with a powerful escape response [43]. These results are in contrast to the finding in Refs. [32,44] that for a squirmer (an imaginary spherical swimmer that deforms its shape tangentially to swim), the optimal configuration for swimming is also optimal for resource acquisition. Obviously, flagellates with more realistic morphology do not necessarily follow this rule, with the haptophytes as a clear example.

2. Basic thrust units

The flagella in biflagellates have two parameters more for the waveform than those of uniflagellates, C_0 and CL_{fl}. With the addition of these two parameters, the material points on the flagellum locally experience a periodic motion around the static component described by $\phi_s(s^*, t) = (CL_{fl})s^* + C_0$ [solid black line in Figs. 1(f) and 1(g)], which makes the flagella relatively closer to the cell body. (See Fig. S8 in the Supplemental Material for the effect of the variation of these two parameters.) If hydrodynamic interactions were negligible, the averaged drag-based thrust of such a waveform locally and spatially would be directed along this static component. In reality, however, hydrodynamic interactions, especially between the flagella and the cell body, are significant. The flagellar beat in biflagellates with short flagella shows a power and return stroke (which happens when $N_w < 1.0$), and this is beneficial for cell swimming and feeding. For the former, it has been previously shown that "hydrodynamic interactions between the flagella and cell body on the return stroke make an important contribution to enhance net forward motion" (Ref. [45], p. 013015-1). For biflagellates with longer flagella (e.g., $L^*_{fl} = 5$), such an effect may still be beneficial to the cell swimming with a power and return stroke (e.g., $N_w = 1.0$), but it deteriorates the cells' feeding performance because flagella would be positioned relatively far from the cell. This may explain why the optimum feeding happens at $N_w = 2.0$, where flagella become relatively closer to the cell body than when, e.g., $N_w = 1.0$. While a further increase in the number of waves may position the flagella closer to the cell body, it decreases the produced thrust of the flagellum, and thus feeding performance deviates from the optimal point.

IV. DISCUSSION AND CONCLUSIONS

Flagellates are arguably the phylogenetically most diverse group of organisms on this planet as they are found in all major branches of the eukaryotic tree of life [46]. They are all characterized by being unicellular and equipped with one or a few flagella that have the same, conserved internal structure shared among all eukaryotes and that play a key role in their ecology. However, flagellates are also functionally diverse, and our findings here demonstrate that to fully understand this diversity, one needs to consider the role of the flagellum beyond propulsion. The variations in flagellar external structure (naked or hairy) and waveform (sinusoidal or nonsinusoidal), as well as additions in the cell morphology (e.g., haptonema), all represent adaptations to fulfill different and specific requirements of the cell.

In free-living nanoflagellates, the flagellum plays the dual role of both producing propulsion and producing the feeding current. Feeding-current generation plays a negligible role in autotrophic cells that rely on the uptake of inorganic nutrient molecules since at these Péclet numbers (Pe < 1) molecular diffusion dominates mass transport. However, propulsion allows the cells to utilize the steep small-scale chemical gradients in the ocean to reach regions of elevated nutrient availability via chemotaxis [6]. In phagotrophic cells that feed on the small nonmotile bacteria that dominate in the open ocean, Brownian diffusion is insufficient to deliver enough prey, and these cells depend on generating an efficient feeding current by means of the flagellum.

However, the activity of the flagellum, whether for propulsion, feeding, or both, always implies a conflict between propulsion and resource acquisition on the one hand and avoiding being eaten on the other. The arrangement, morphology, and beat pattern of the flagellum may or may not accentuate this conflict. In uniflagellates with a naked flagellum that pushes the cell forward, the optimum waveform for propulsion and stealth appears to be the same. Among free-living flagellates, this configuration is only found among animal sperm and nonfeeding swarmer stages of the otherwise purely phagotrophic choanoflagellates (a sister group to animals). The flagellum may in choanoflagellates be equipped with a vane that enhances the swimming performance but that does not otherwise change the design requirements. Neither sperm nor swarmer stages of choanoflagellates acquire resources, and such uniflagellates would, in fact, also be very inefficient foragers [Fig. 5(d)]. When choanoflagellates feed, the cell forms a collar filter around the flagellum, and the beating flagellum drives a flow of water through the collar where bacterial prey is strained. The constriction of the flagellum within a collar and the presence of a vane on the flagellum together make the force generated by the flagellum sufficient to drive an efficient feeding current through the fine-meshed collar filter [24]. Many other flagellates, in fact, have a flagellum equipped with a vane (or similar) and embedded in a groove or other constriction on the cell surface, for example, dinoflagellates [47] and excavates [48]. Such an arrangement is conducive to the efficient generation of feeding current but not adapted for efficient swimming.

Other functionally uniflagellated flagellates are the heterokont alveolates, where the active flagellum is equipped with hairs (the second flagellum plays no role in propulsion and feeding-current generation), increasing the thrust production by a factor of 5–10 and allowing an efficient incoming feeding current [23,24]. The heterokont alveolates appear to be the dominant phagotrophic nanoflagellates in the ocean [49,50], and according to our analyses, they appear also to be the most efficient grazers [Figs. 2(f), 5(d), and 5(e)] on nonmotile bacteria. Here, however, there is a design conflict between foraging and propulsion and stealth: The more efficient grazers also run the highest risk of being perceived by a flow-sensing predator and are the poorest swimmers. Different environments, whether rich in predators or rich in bacterial prey, may balance this trade-off differently, giving rise to different forms (species) dominating in different areas and at different seasons and, thus, to biodiversity.

Among the biflagellates we find a similar pattern: In the autotrophic (or predominantly autotrophic) biflagellates, optimality for propulsion and foraging requirements conflicts

weakly with stealth, while in the haptophytes with long flagella and a long prey-collecting haptonema, optimal design for propulsion and stealth conflicts with foraging requirements. This trade-off is further accentuated by the presence of the haptonema that adds drag and produces noise but increases feeding efficiency. The observed flagellar waveforms differ between the three model species, but all are near the optimal for foraging [Fig. 5(d)]. The biflagellates are all more efficient grazers than the naked uniflagellates, and the haptophytes are more efficient than the biflagellates without a haptonema. This is consistent with the observation that the most efficient mixotrophic biflagellates in the ocean are found among the haptophytes [51].

We have here covered only uni- and biflagellated cells, while in the ocean one finds forms with 4, 8, and 16 flagella organized similarly to the biflagellates considered here, i.e., in couples arranged across one another, beating synchronously or not. These are likely to have optimality criteria that are very similar to but different from those of the biflagellates considered here. Other flagellates again have three-dimensional beat patterns rather than the simple planar beats, and this may lead to quite different optimalities and, hence, design trade-offs. However, three-dimensional beat patterns have to our knowledge only been described in any detail for *Euglena gracilis* [52]. Exploring the design optima and implications of three-dimensional beat patterns would help further our understanding of the vast diversity of flagellar arrangements found in free-living flagellates.

ACKNOWLEDGMENTS

We received funding from the Independent Research Fund Denmark (7014-00033B), the Carlsberg Foundation (CF17-0495), and the Simons Foundation (931976). The Centre for Ocean Life is supported by the Villum Foundation.

[1] F. Azam, T. Fenchel, J. G. Field, J. S. Gray, L. A. Meyer-Reil, and F. Thingstad, The ecological role of water-column microbes in the sea, Mar. Ecol. Prog. Ser. **10**, 257 (1983).

[2] A. Z. Worden, M. J. Follows, S. J. Giovannoni, S. Wilken, A. E. Zimmerman, and P. J. Keeling, Rethinking the marine carbon cycle: Factoring in the multifarious lifestyles of microbes, Science **347**, 1257594 (2015).

[3] T. Weisse, R. Anderson, H. Arndt, A. Calbet, P. J. Hansen, and D. J. S. Montagnes, Functional ecology of aquatic phagotrophic protists–concepts, limitations, and perspectives, Eur. J. Protistol. **55**, 50 (2016).

[4] C. Bachy, E. Hehenberger, Y.-C. Ling, D. M. Needham, J. Strauss, S. Wilken, and A. Z. Worden, Marine protists: A hitchhiker's guide to their role in the marine microbiome, in *The Marine Microbiome* (Springer, New York, 2022), pp. 159–241.

[5] T. Fenchel, Ecology of heterotrophic microflagellates. I. Some important forms and their functional morphology, Mar. Ecol. Prog. Ser. **8**, 211 (1982).

[6] R. Stocker, Marine microbes see a sea of gradients, Science **338**, 628 (2012).

[7] T. Kiørboe, H. Jiang, R. J. Gonçalves, L. T. Nielsen, and N. Wadhwa, Flow disturbances generated by feeding and swimming zooplankton, Proc. Natl. Acad. Sci. USA **111**, 11738 (2014).

[8] Ø. Moestrup, Flagellar structure in algae: A review, with new observations particularly on the *Chrysophyceae, Phaeophyceae (Fucophyceae), Euglenophyceae*, and *Reckertia*, Phycologia **21**, 427 (1982).

[9] J. L. Mah, K. K. Christensen-Dalsgaard, and S. P. Leys, Choanoflagellate and choanocyte collar-flagellar systems and the assumption of homology, Evol. Dev. **16**, 25 (2014).

[10] L. T. Nielsen and T. Kiørboe, Foraging trade-offs, flagellar arrangements, and flow architecture of planktonic protists, Proc. Natl. Acad. Sci. USA **118**, e2009930118 (2021).

[11] S. S. Asadzadeh, L. T. Nielsen, J. Dölger, A. Andersen, T. Kiørboe, P. S. Larsen, and J. H. Walther, Hydrodynamic functionality of the lorica in choanoflagellates, J. R. Soc. Interface **16**, 20180478 (2019).

[12] J. S. Guasto, R. Rusconi, and R. Stocker, Fluid mechanics of planktonic microorganisms, Annu. Rev. Fluid Mech. **44**, 373 (2012).

[13] E. Lauga and T. R. Powers, The hydrodynamics of swimming microorganisms, Rep. Prog. Phys. **72**, 096601 (2009).

[14] E. Lauga and C. Eloy, Shape of optimal active flagella, J. Fluid Mech. **730**, R1 (2013).

[15] T. Fenchel, The ecology of heterotrophic microflagellates, in *Advances in Microbial Ecology*, Advances in Microbial Ecology Series Vol. 9 (Springer, New York, 1986), pp. 57–97.

[16] T. Kiørboe, Fluid dynamic constraints on resource acquisition in small pelagic organisms, Eur. Phys. J.: Spec. Top. **225**, 669 (2016).

[17] V. F. Geyer, J. Howard, and P. Sartori, Ciliary beating patterns map onto a low-dimensional behavioural space, Nat. Phys. **18**, 332 (2022).

[18] S. Suzuki-Tellier, A. Andersen, and T. Kiørboe, Mechanisms and fluid dynamics of foraging in heterotrophic nanoflagellates, Limnol. Oceanogr. **67**, 1287 (2022).

[19] G. B. Bouck, The structure, origin, isolation, and composition of the tubular mastigonemes of the *Ochromonas* flagellum, J. Cell Biol. **50**, 362 (1971).

[20] M. A. Sleigh, Flagellar movement of the sessile flagellates *Actinomonas, Codonosiga, Monas*, and *Poteriodendron*, J. Cell Sci. **s3-105**, 405 (1964).

[21] T. L. Jahn, M. D. Lanoman, and J. R. Fonseca, The mechanism of locomotion of flagellates. II. Function of the mastigonemes of *Ochromonas*, J. Protozool. **11**, 291 (1964).

[22] M. A. Sleigh, Mechanisms of flagellar propulsion, Protoplasma **164**, 45 (1991).

[23] S. S. Asadzadeh, J. H. Walther, A. Andersen, and T. Kiørboe, Hydrodynamic interactions are key in thrust-generation of hairy flagella, Phys. Rev. Fluids **7**, 073101 (2022).

[24] L. T. Nielsen, S. S. Asadzadeh, J. Dölger, J. H. Walther, T. Kiørboe, and A. Andersen, Hydrodynamics of microbial filter feeding, Proc. Natl. Acad. Sci. USA **114**, 9373 (2017).

[25] S. S. Asadzadeh, T. Kiørboe, P. S. Larsen, S. P. Leys, G. Yahei, and J. H. Walther, Hydrodynamics of sponge pumps

and evolution of the sponge body plan, eLIFE **9**, e61012 (2020).

[26] G. J. Amador, D. Wei, D. Tam, and M.-E. Aubin-Tam, Fibrous flagellar hairs of *Chlamydomonas reinhardtii* do not enhance swimming, Biophys. J. **118**, 2914 (2020).

[27] V. F. Geyer, P. Sartori, B. M. Friedrich, F. Jülicher, and J. Howard, Independent control of the static and dynamic components of the *Chlamydomonas* flagellar beat, Curr. Biol. **26**, 1098 (2016).

[28] See Supplemental Material at http://link.aps.org/supplemental/10.1103/PRXLife.1.013002 for the details of the beat analysis for biflagellate model organisms, the dimensional analysis, and the effect of some input parameters on the output parameters.

[29] B. S. C. Leadbeater, The 'mystery' of the flagellar vane in choanoflagellates, Nova Hedwigia Beih. **130**, 213 (2006).

[30] M. Dayel, R. Alegado, S. Fairclough, T. Levin, S. Nichols, K. McDonald, and N. King, Cell differentiation and morphogenesis in the colony-forming choanoflagellate *Salpingoeca rosetta*, Dev. Biol. **357**, 73 (2011).

[31] T. Kiørboe and A. G. Hirst, Shifts in mass scaling of respiration, feeding, and growth rates across life-form transitions in marine pelagic organisms, Am. Nat. **183**, E118 (2014).

[32] S. Michelin and E. Lauga, Optimal feeding is optimal swimming for all Péclet numbers, Phys. Fluids **23**, 101901 (2011).

[33] D. Tam and A. E. Hosoi, Optimal kinematics and morphologies for spermatozoa, Phys. Rev. E **83**, 045303(R) (2011).

[34] H. Nguyen, M. A. R. Koehl, C. Oakes, G. Bustamante, and L. Fauci, Effects of cell morphology and attachment to a surface on the hydrodynamic performance of unicellular choanoflagellates, J. R. Soc. Interface **16**, 20180736 (2019).

[35] D. Tam and A. E. Hosoi, Optimal feeding and swimming gaits of biflagellated organisms, Proc. Natl. Acad. Sci. USA **108**, 1001 (2011).

[36] B. Rodenborn, C.-H. Chen, H. L. Swinney, B. Liu, and H. P. Zhang, Propulsion of microorganisms by a helical flagellum, Proc. Natl. Acad. Sci. USA **110**, E338 (2013).

[37] S. S. Asadzadeh, P. S. Larsen, H. U. Riisgård, and J. H. Walther, Hydrodynamics of the leucon sponge pump, J. R. Soc. Interface **16**, 20180630 (2019).

[38] P. Sartori, V. F. Geyer, A. Scholich, F. Jülicher, and J. Howard, Dynamic curvature regulation accounts for the symmetric and asymmetric beats of *Chlamydomonas* flagella, eLIFE **5**, e13258 (2016).

[39] Y. Hara and M. Chihara, Ultrastructure and taxonomy of *Fibrocapsa japonica* (class raphidophyceae), Arch. Protistenkd. **130**, 133 (1985).

[40] C. Eloy and E. Lauga, Kinematics of the Most Efficient Cilium, Phys. Rev. Lett. **109**, 038101 (2012).

[41] M. Kawachi, I. Inouye, O. Maeda, and M. Chihara, The haptonema as a food-capturing device: Observations on *Chrysochromulina hirta (Prymnesiophyceae)*, Phycologia **30**, 563 (1991).

[42] M. Nomura, K. Atsuji, K. Hirose, K. Shiba, R. Yanase, T. Nakayama, K.-i. Ishida, and K. Inaba, Microtubule stabilizer reveals requirement of Ca^{2+}-dependent conformational changes of microtubules for rapid coiling of haptonema in haptophyte algae, Biol. Open **8**, bio.036590 (2019).

[43] H. H. Jakobsen, Escape of protists in predator-generated feeding currents, Aquat. Microb. Ecol. **26**, 271 (2002).

[44] S. Michelin and E. Lauga, Unsteady feeding and optimal strokes of model ciliates, J. Fluid Mech. **715**, 1 (2013).

[45] H. Kurtuldu, D. Tam, A. E. Hosoi, K. A. Johnson, and J. P. Gollub, Flagellar waveform dynamics of freely swimming algal cells, Phys. Rev. E **88**, 013015 (2013).

[46] D. V. Tikhonenkov, Predatory flagellates – the new recently discovered deep branches of the eukaryotic tree and their evolutionary and ecological significance, Protistology **14**, 15 (2020).

[47] L. T. Nielsen and T. Kiørboe, Feeding currents facilitate a mixotrophic way of life, ISME J. **9**, 2117 (2015).

[48] T. Pánek, P. Táborský, M. G. Pachiadaki, M. Hroudová, Č. Vlček, V. P. Edgcomb, and I. Čepička, Combined culture-based and culture-independent approaches provide insights into diversity of jakobids, an extremely plesiomorphic eukaryotic lineageukaryotic tree and their evolutionary and ecological significance, Front. Microbiol. **6**, 1288 (2015).

[49] A. Obiol, I. Muhovic, and R. Massana, Oceanic heterotrophic flagellates are dominated by a few widespread taxa, Limnol. Oceanogr. **66**, 4240 (2021).

[50] N. A. Kamennaya, G. Kennaway, M. A. Sleigh, and M. V. Zubkov, Notable predominant morphology of the smallest most abundant protozoa of the open ocean revealed by electron microscopy, J. Plankton Res. **44**, 542 (2022).

[51] Q. Li, K. F. Edwards, C. R. Schvarcz, and G. F. Steward, Broad phylogenetic and functional diversity among mixotrophic consumers of *Prochlorococcus*, ISME J. **16**, 1557 (2022).

[52] M. Rossi, G. Cicconofri, A. Beran, G. Noselli, and A. DeSimone, Kinematics of flagellar swimming in *Euglena gracilis*: Helical trajectories and flagellar shapes, Proc. Natl. Acad. Sci. USA **114**, 13085 (2017).